A WAVE2–Arp2/3 actin nucleator apparatus supports junctional tension at the epithelial zonula adherens

Suzie Verma[a], Siew Ping Han[a], Magdalene Michael[a], Guillermo A. Gomez[a], Zhe Yang[a], Rohan D. Teasdale[a], Aparna Ratheesh[a], Eva M. Kovacs[a], Radiya G. Ali[a,b], and Alpha S. Yap[a]
[a]Division of Molecular Cell Biology, Institute for Molecular Bioscience, and [b]School for Biomedical Sciences, University of Queensland, St. Lucia, Brisbane 4072, Australia

ABSTRACT **The epithelial zonula adherens (ZA) is a specialized adhesive junction where actin dynamics and myosin-driven contractility coincide. The junctional cytoskeleton is enriched in myosin II, which generates contractile force to support junctional tension. It is also enriched in dynamic actin filaments, which are replenished by ongoing actin assembly. In this study we sought to pursue the relationship between actin assembly and junctional contractility. We demonstrate that WAVE2–Arp2/3 is a major nucleator of actin assembly at the ZA and likely acts in response to junctional Rac signaling. Furthermore, WAVE2–Arp2/3 is necessary for junctional integrity and contractile tension at the ZA. Maneuvers that disrupt the function of either WAVE2 or Arp2/3 reduced junctional tension and compromised the ability of cells to buffer side-to-side forces acting on the ZA. WAVE2–Arp2/3 disruption depleted junctions of both myosin IIA and IIB, suggesting that dynamic actin assembly may support junctional tension by facilitating the local recruitment of myosin.**

Monitoring Editor
Jeffrey D. Hardin
University of Wisconsin

Received: Aug 6, 2012
Revised: Sep 27, 2012
Accepted: Oct 2, 2012

INTRODUCTION

The epithelial zonula adherens (ZA) is a specialized adhesive junction implicated in tissue integrity and apical contractility (Sawyer *et al.*, 2010). It is characterized by the local accumulation of E-cadherin in a ring-like zone at the apical–lateral interface between cells (Tepass and Hartenstein, 1994; Muller and Wieschaus, 1996; Otani *et al.*, 2006; Kovacs *et al.*, 2011). This lies contiguous to concentrations of F-actin that have been reported to organize into dense bundles (Hirokawa *et al.*, 1983; Tepass and Hartenstein, 1994). The ZA is a site where adhesion is coordinated with contractile forces, which combine to generate tension in the junction (Fernandez-Gonzalez *et al.*, 2009; Ratheesh *et al.*, 2012). Consistent with this, the apical actin ring is enriched in myosin II (Ivanov *et al.*, 2005; Smutny *et al.*, 2010), the major contractile tension generator within cells, and disruption of myosin II or its upstream activators perturbs ZA integrity (Smutny *et al.*, 2010; Ratheesh *et al.*, 2012). Junctional tension in the ZA may contribute to morphogenesis of epithelial sheets (Loveless and Hardin, 2012), orient cells within tissues (Fernandez-Gonzalez *et al.*, 2009), and allow the ZA to resist side-to-side (orthogonal) forces (Smutny *et al.*, 2011).

Myosin II generates contractile force by binding to, and sliding, actin filaments (Vicente-Manzanares *et al.*, 2009). Self-assembly of individual myosins into antiparallel minifilaments allows plus end–directed motor activity to slide filaments in networks toward one another (Verkhovsky *et al.*, 1995; Clark *et al.*, 2007). This also implies that properties of their interacting actin filaments can influence myosin II–driven contractility. Indeed, actin filament geometry and polarity have recently been demonstrated to affect contractility (Reymann *et al.*, 2012). An important potential determinant of actin network geometry is the molecular mechanism responsible for mediating nucleation, the rate-limiting step in actin assembly (Michelot and Drubin, 2011). Thus the Arp2/3 complex nucleates the assembly of branched actin networks, whereas formin-based nucleation generates unbranched filaments. Of interest, Arp2/3 activity appears to limit the action of myosin in generating retrograde actin flow (Yang *et al.*, 2012). Furthermore, type II myosins in yeast tend to segregate toward formin-derived linear actin filament arrays

This article was published online ahead of print in MBoC in Press (http://www.molbiolcell.org/cgi/doi/10.1091/mbc.E12-08-0574) on October 10, 2012.

Address correspondence to: Alpha S. Yap (a.yap@uq.edu.au).

Abbreviations used: AU, arbitrary units; DN, dominant-negative; FRAP, fluorescence recovery after photobleaching; IP, immunoprecipitation; LatA, latrunculin A; WRC, WAVE regulatory complex; ZA, zonula adherens; ZO-1, zonula occludens protein 1.

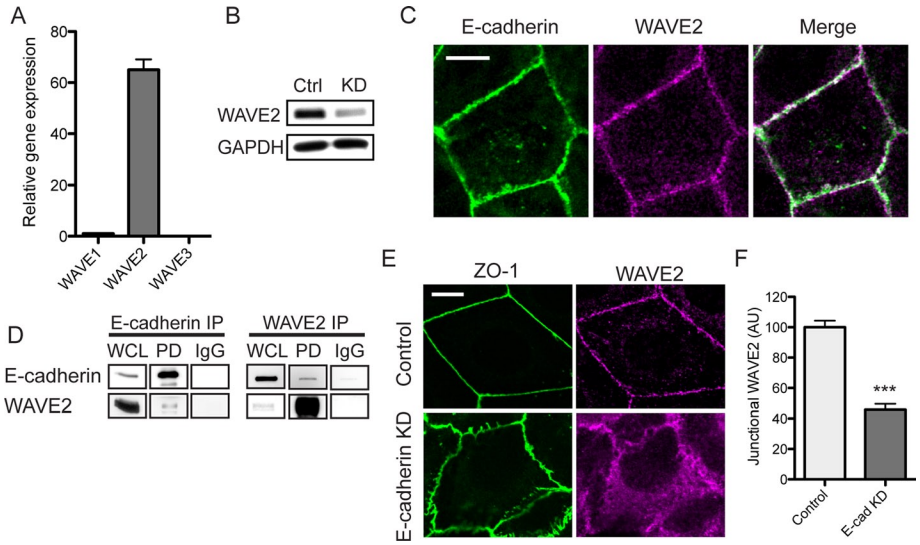

FIGURE 1: WAVE2 is a junctional component at the zonula adherens. (A) Relative mRNA transcript levels of WAVE proteins in Caco-2 cells, $n = 7$. (B) Validation of WAVE2 knockdown and antibody specificity. Lysates from control (Ctrl) and WAVE2 siRNA (KD) cells were immunoblotted for WAVE2. Results are representative of three independent experiments. (C) E-cadherin and WAVE2 colocalized at the zonula adherens. Confluent Caco-2 monolayers were stained for E-cadherin and WAVE2 by indirect immunofluorescence. (D) Coimmunoprecipitation (IP) of E-cadherin and WAVE2. Immunoglobulin G was used as a control. Results are representative of two independent experiments. PD, pull down; WCL, whole-cell lysate. (E) Junctional WAVE2 is reduced in E-cadherin knockdown, although tight junctions remained intact, as revealed by ZO-1 staining. (F) Junctional WAVE2 in control and E-cadherin knockdown (E-cad KD) cells quantified by line scan analysis; $n = 10$ contacts for control and 15 contacts for KD from three independent experiments. Scale bars, 10 μm. ***$p < 0.001$; data are means ± SEM, normalized to controls; AU, arbitrary units.

rather than Arp2/3-nucleated actin networks (Michelot and Drubin, 2011).

Both Arp2/3 and formins have been implicated in actin regulation at cadherin junctions. In recent work (Kovacs *et al.*, 2011), we identified two pools of actin at the ZA, as were also seen in other systems (Zhang *et al.*, 2005). The most prominent were apical rings (Kovacs *et al.*, 2011) that also label for myosin II (Smutny *et al.*, 2010) and potentially comprise bundled filaments (Hirokawa *et al.*, 1983; Tepass and Hartenstein, 1994). In addition, a cortical pool was seen at the junctional membrane that was spatially distinguishable from the apical actin rings (Kovacs *et al.*, 2011). This cortical pool marked the major site for actin nucleation at the ZA, as measured by labeling for actin barbed ends, and localized with Arp2/3 (Kovacs *et al.*, 2011). Furthermore, nucleation was substantially reduced by drug inhibitors of Arp2/3. Surprisingly, however, inhibition of Arp2/3 depleted both the cortical actin pool and the perijunctional actin rings. This suggested that these morphologically distinct pools might be coupled and further implied that Arp2/3 contributed to generating much of the cytoskeleton at the ZA. What effect this might have on junctional tension, however, was unclear.

Arp2/3 does not, however, initiate actin assembly in isolation. It is activated in response to cell signaling by a number of intermediary proteins, of which the best understood are the WASP/WAVE family of nucleation-promoting factors (Padrick and Rosen, 2010). In mammalian cells these include three WAVE proteins, WASP, and N-WASP. All bear a conserved C-terminal VCA domain that binds to, and activates, Arp2/3. WASP/WAVE proteins often control the site-specific activity of Arp2/3 (Berger *et al.*, 2008). For example, WASP proteins are implicated in activating Arp2/3 during clathrin-mediated endocytosis (Weinberg and Drubin, 2012), whereas WAVE proteins act at the leading edges of lamellipodia (Steffen *et al.*, 2004). Which of these might be responsible for activating Arp2/3 at the ZA is less clear. Both N-WASP and WAVE have been identified at cadherin-based cell–cell junctions (Ivanov *et al.*, 2005; Yamazaki *et al.*, 2007; Kovacs *et al.*, 2011), but we recently demonstrated that N-WASP does not activate Arp2/3 there and instead regulates the junctional cytoskeleton at a postnucleation stage (Kovacs *et al.*, 2011). Therefore in this study we aimed to clarify the role of WAVE in junctional actin regulation as the basis for testing the effect of Arp2/3-mediated nucleation upon force generation at the ZA.

RESULTS

WAVE2 is a component of the zonula adherens

We performed our studies in Caco-2 colon epithelial cells, a cell line that forms simple polarized monolayers with prominent ZAs at their cell–cell junctions. Quantitative real-time PCR revealed that WAVE2 was the predominant form expressed in these cells; only trace WAVE1 signals were identified, and WAVE3 was essentially undetectable (Figure 1A). The expression of WAVE2 protein in Caco-2 cells was confirmed by immunoblotting, which showed a single polypeptide band that was substantially reduced by small interfering RNA (siRNA), confirming the specificity of the antibody (Figure 1B).

Confocal immunofluorescence microscopy demonstrated clear junctional staining for WAVE2, which coaccumulated with E-cadherin at the apical ring of the ZA (Figure 1C). WAVE2 staining was largely abolished by siRNA, supporting the specificity of the ZA staining pattern (Supplemental Figure S1A), which was further corroborated by localization of WAVE2-mCherry with E-cadherin at apical cell–cell contacts (Supplemental Figure S1B).

Taken together, these findings identify WAVE2 as a component of the epithelial ZA. Consistent with this, we found that E-cadherin and WAVE2 coimmunoprecipitate (Figure 1D). Furthermore, E-cadherin was necessary for WAVE2 to localize to junctions, as WAVE2 staining at cell–cell contacts was substantially reduced when E-cadherin was depleted by siRNA (Figure 1, E and F). Note that E-cadherin RNA interference (RNAi) cells remained in contact with one another, as ZO-1 staining revealed the persistence of tight junctions, albeit with altered morphology. Overall these observations suggest that WAVE2 is recruited to the ZA in response to E-cadherin adhesion.

Rac GTPase signaling regulates junctional WAVE2

WASP/WAVE proteins can be regulated by the Rho-family GTPases Rac and Cdc42. In particular, WAVE has commonly been identified as a downstream target of Rac (Steffen *et al.*, 2004; Insall and Machesky, 2009; Padrick and Rosen, 2010), and both Rac and Cdc42 can mediate E-cadherin signaling (Kim *et al.*, 2000; Kraemer *et al.*, 2007). Indeed both Rac (Figure 2A) and Cdc42 (Figure 2B) coaccumulated with WAVE2 at the ZA. We then expressed dominant-negative (DN) mutants of Rac (N17) and Cdc42 (N17) in Caco-2 cells and

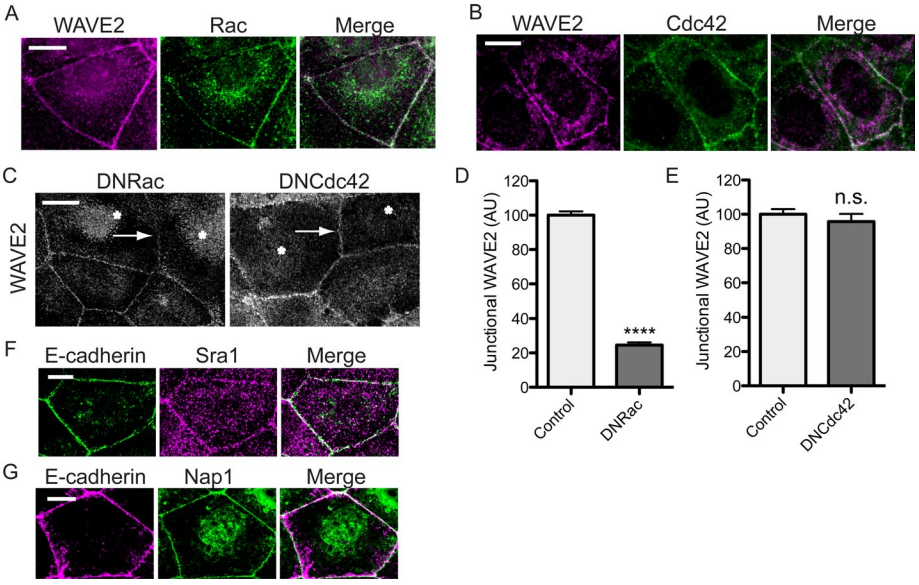

FIGURE 2: Rac signaling regulates junctional WAVE2. (A, B) Rac and Cdc42 coaccumulate with WAVE2 at the zonula adherens. Caco-2 cells were immunostained for WAVE2 and either Rac (A) or Cdc42 (B) and imaged by confocal microscopy. (C–E) Junctional WAVE2 requires Rac signaling. Caco-2 cells transiently expressing dominant-negative (DN) Rac or DN Cdc42 mutants were immunostained for WAVE2 and the epitope tag (not shown). Asterisks mark cells positive for DN-Rac or DN-Cdc42 expression, and arrows indicate contacts between transgene-expressing cells. Junctional WAVE2 was reduced at contacts between cells expressing DN-Rac but not at contacts between cells expressing DN-Cdc42 (D, E; $n = 30$ contacts from three independent experiments each; data are means ± SEM, normalized to control. $^{****}p < 0.0001$; n.s. not significant; AU, arbitrary units). (F, G) WAVE regulatory complex components are junctional proteins. Confluent Caco-2 monolayers were costained for E-cadherin and either Sra1 (F) or Nap1 (G) and imaged at the ZA. Scale bars, 10 μm.

examined their effect on junctional WAVE2. DN-Rac, but not DN-Cdc42, significantly reduced WAVE2 localization at the ZA (Figure 2, C–E), evidence that WAVE2 might localize to the ZA in response to Rac. WAVE proteins do not, however, possess GTPase-binding domains, their activation being mediated by intermediary proteins, notably the multimeric WAVE regulatory complex (WRC; Steffen *et al.*, 2004; Padrick and Rosen, 2010). Indeed, both Sra1 and Nap1, components of the WRC, localized to junctions (Figure 2, F and G), suggesting that junctional WAVE2 might act as part of the WRC.

WAVE2 regulates junctional actin assembly

On close inspection, WAVE2 was seen to stain at the junctional cortex (Figure 3A), its peak fluorescence typically lying between the apical actin rings (Figure 3B). This corresponds to the principal site of barbed-end labeling (Kovacs *et al.*, 2011). Furthermore, WAVE2 colocalized with the Arp3 component of the Arp2/3 complex (Figure 3C). To assess actin nucleation at the ZA, we briefly incubated saponin-permeabilized cells with Alexa 594–labeled G-actin used at a concentration that preferentially labels the actin filament barbed ends (Kovacs *et al.*, 2011). Cells were costained with phalloidin to assess steady-state junctional F-actin. In control Caco-2 cells, G-actin principally labeled at the junctional membrane of the ZA (Figure 3F). Both barbed-end labeling and the steady-state F-actin content of the ZA were reduced in cells transfected with Arp3 siRNA (Figure 3, F and G). The decrease in junctional F-actin encompassed both the cortical pools and the apical actin rings. Taken together with our recent experience using small-molecule inhibitors (Kovacs *et al.*, 2011), this confirms that Arp2/3 is a major nucleator of actin assembly at the ZA.

Both barbed-end labeling and steady-state F-actin levels were also reduced in WAVE2 KD cells compared with cells transfected with control siRNA (Figure 3, F and G). Here we used an siRNA SmartPool, which reduced WAVE2 levels by ~60% (Figure 1B). The reduction in phalloidin staining in these saponin-treated cells was comparable to that seen in cells that were stained after standard fixation without prior saponin permeabilization (not shown). Steady-state junctional F-actin was also reduced when WAVE2 was depleted with an siRNA directed against the 3′ untranslated region (UTR) and restored by expression of an RNAi-resistant WAVE2–green fluorescent protein (GFP) transgene (Supplemental Figure S2), confirming that the effect of the siRNA was due to WAVE2 depletion. Furthermore, junctional staining for Arp3 was significantly reduced in WAVE2 KD cells (Figure 3, D and E), consistent with the notion that WAVE2 functions upstream of Arp2/3 in junctional actin regulation.

As an independent test of actin assembly at cadherin junctions, we examined how the junctional cytoskeleton was affected upon addition, and then washout, of latrunculin, an approach recently introduced by Tang and Brieher (2012). As reported in Madin–Darby canine kidney (MDCK) cells (Tang and Brieher, 2012), latrunculin substantially reduced steady-state F-actin at junctions. F-actin pools at the junctional cortex and in apical rings were largely abolished, replaced by residual puncta of F-actin that also stained for WAVE2 and Arp2/3 (Figure 4A). After removal of latrunculin, puncta were progressively replaced by a more diffuse phalloidin pattern. With time, the junctional region was repopulated by F-actin, initially appearing loosely packed at the cortex and eventually organizing to form apical actin rings. WAVE2 was also recruited to junctions, first in puncta and then distributing throughout an apical junctional ring (Figure 4A). However, the F-actin content was consistently reduced in the WAVE2 KD cells (Figure 4B,C), as was the rate of initial recovery after removal of latrunculin (unpublished data). Moreover, F-actin filaments at the junctions remained disorganized in the WAVE2 KD cells, even 60 min after latrunculin washout. This further supported the notion that WAVE2 contributes to junctional actin assembly.

WAVE2 supports ZA integrity and junctional dynamics of E-cadherin

WAVE2 depletion dramatically altered the integrity of the zonula adherens. E-cadherin staining intensity was reduced, and the ring-like organization of apical E-cadherin seen in control cells appeared fragmented in WAVE2 KD cells, being often interrupted by discontinuities (Figure 5, A and B). This alteration in E-cadherin staining at the ZA was not due to an overall change in cadherin expression: immunoblotting showed that total levels of E-cadherin were similar in control and WAVE2 KD cells (Figure 5C). Furthermore, trypsin-sensitivity assays (Takeichi, 1977; Yap *et al.*, 1997) demonstrated that surface levels of E-cadherin were similar in the two cell lines. In control cells the majority of cellular cadherin was accessible to

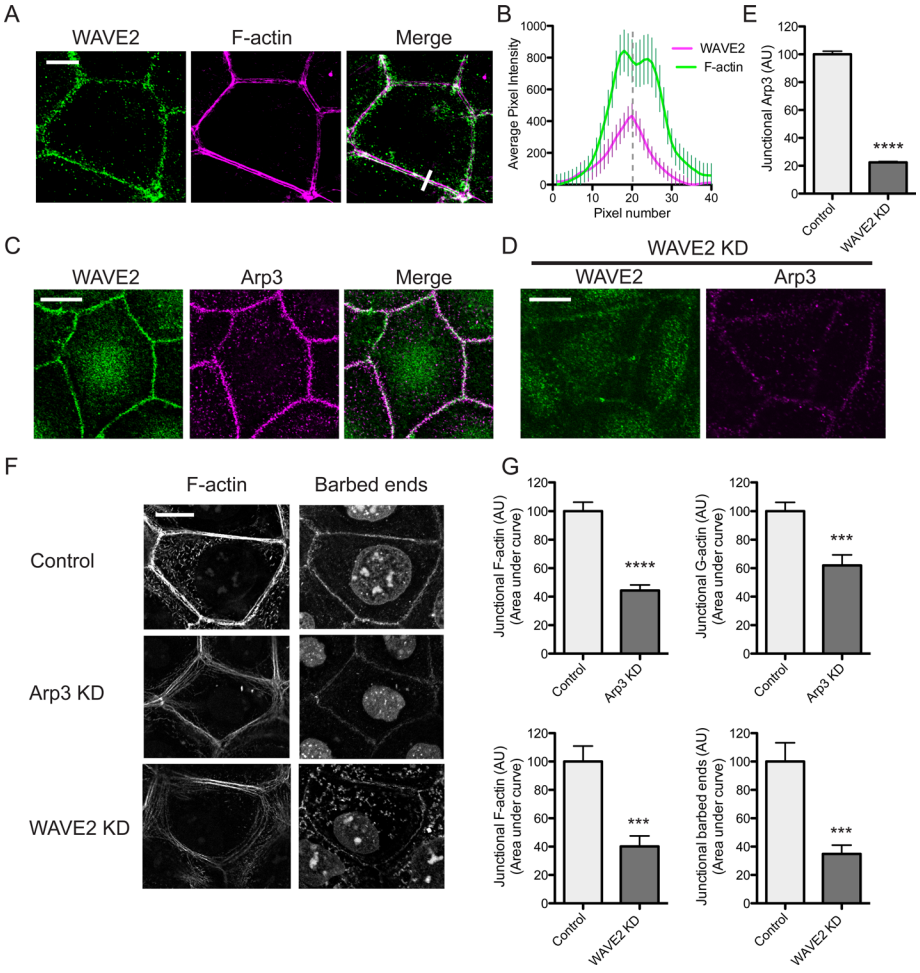

FIGURE 3: WAVE2 regulates junctional actin assembly. (A, B) WAVE2 localized at the ZA between apical F-actin rings. WAVE2 and F-actin were visualized by confocal immunofluorescence imaging (A) and the fluorescence profiles measured by line scan analysis of 20 contacts (B). A representative line scan is marked by a white bar in the merged image in A. (C) Coaccumulation of WAVE2 and Arp3 at the ZA imaged by confocal immunofluorescence microscopy. (D, E) Junctional Arp3 is depleted in WAVE2 RNAi cells. Control and WAVE2 siRNA cells were immunostained for WAVE2 and Arp3. Costaining in WAVE2 KD cells is shown in D and junctional Arp3 quantitated by line scan analysis in control and WAVE2 KD cells in (E; $n = 40$ contacts from three independent experiments). (F, G) Junctional actin nucleation and F-actin are perturbed in Arp3 and WAVE2 RNAi cells. Barbed ends and junctional F-actin were labeled by incorporation of Alexa 594 G-actin and phalloidin staining, respectively, in control, Arp3 siRNA, and WAVE2 siRNA cells. Representative images are shown in F and quantitation in G. Data are $n = 24$ for control and $n = 24$ for Arp3 siRNA; $n = 15$ contacts for control and $n = 13$ contacts for WAVE2 siRNA from three independent experiments. ***$p < 0.001$; ****$p < 0.0001$; data are means ± SEM, normalized to control; AU, arbitrary units. Scale bars, 10 μm.

surface trypsinization in the absence of Ca^{2+}, and this was not altered in WAVE2 KD cells (Figure 5C). This suggested that the steady-state balance between surface and internal cadherin pools was not affected by WAVE2 KD.

Instead, we considered the possibility that surface dynamics of cadherin was influenced by WAVE2. Accordingly, we measured fluorescence recovery after photobleaching (FRAP) of apical junctional E-cadherin-GFP expressed by lentiviral transduction in E-cadherin KD cells (Figure 5D; Smutny *et al.*, 2011). FRAP data were well fitted to a monoexponential function that showed reduction in both the $T_{1/2}$ of recovery (Figure 5E) and mobile fraction in WAVE2 KD cells (Figure 5F). This suggested that a mobile pool of surface E-cadherin might depend on WAVE2 function.

In contrast to the alteration in E-cadherin staining, ZO-1 remained detectable at apical junctions, and the fluorescence intensity of ZO-1 was unchanged in WAVE KD cells (Figure 5G). Morphologically, however, ZO-1 staining was more irregular and less linear in the WAVE2 KD cells than in controls, an appearance that was confirmed by quantitating junctional linearity (Figure 5H; Otani *et al.*, 2006). Overall this implies that WAVE2 has a relatively selective effect to support ZA integrity, with more subtle morphological effects on tight junctions.

WAVE2 and Arp2/3 are necessary for junctional tension in the zonula adherens

The linear morphology of tight junctions is often interpreted as an index of apical junctional tension (Otani *et al.*, 2006). Thus the altered linearity in ZO-1 staining suggested that WAVE2 depletion might reduce apical junctional tension. We also observed that E-cadherin–GFP at apical junctions shows increased side-to-side (orthogonal) movements when myosin II is depleted (Smutny *et al.*, 2011) and, by implication, junctional tension is reduced (Ratheesh *et al.*, 2012). Accordingly, we then examined the effect of WAVE2 depletion on apical E-cadherin–GFP movement in time-lapse movies (Figure 6, A–C, and Supplemental Movies S1 and S2). Apical junctions in control cells, reflecting the ZA, were relatively stable, and kymographs showed minimal orthogonal fluctuations in the *xy*-plane. In contrast, WAVE2 KD cells displayed much more dramatic side-to-side movements, as evident in a comparison of kymographs of junctional movement (Figure 6A). We characterized these further by Fourier analysis (Smutny *et al.*, 2011), which revealed increased power in both lower- and higher-frequency peaks, consistent with increased movement (Figure 6B). Earlier we found that changes in low-frequency power in these Fourier analyses reflected slow, unidirectional movement of the junctions from one side to the other (Smutny *et al.*, 2011). Consistent with this, we found that overall translocation of junctions, measured by the slope of the kymographs, was increased in WAVE2 KD cells (Figure 6C). Thus WAVE2 contributes to buffering apical junctions from side-to-side movements.

Then we directly tested the effect of WAVE2 on junctional tension by using a femtosecond laser to cut junctions (Fernandez-Gonzalez *et al.*, 2009) and measuring the instantaneous rate of recoil of their vertices as an index of junctional tension (Ratheesh *et al.*, 2012; Figure 6D). Control junctions displayed rapid recoil of their vertices when junctional integrity was cut by the laser nanoscissors. In contrast, both instantaneous rate of recoil (indicating tension) and the degree of recoil were reduced by WAVE2 KD (Figure 6, E and F). This suggested that WAVE2-mediated actin assembly might

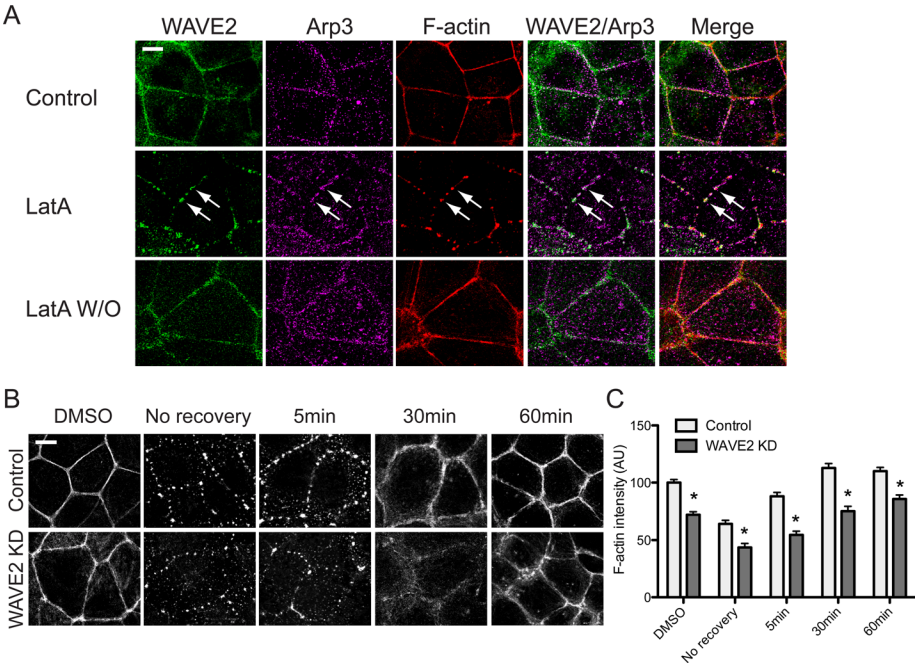

FIGURE 4: WAVE2 is required for actin reassembly. (A) Staining for WAVE2, Arp3, and F-actin during reassembly of the junctional actin cytoskeleton. Caco-2 monolayers were examined after treatment with dimethyl sulfoxide (DMSO) alone (Control), with latrunculin A (LatA; 1 μM, 2 h), or 1 h after washout of latrunculin (LatA W/O). WAVE2, Arp3, and F-actin were visualized by confocal immunofluorescence imaging. WAVE2 and Arp3 colocalized with LatA-resistant F-actin puncta (middle row, arrows). Within 60 min of recovery, WAVE2 and Arp3 had redistributed along the apical actin rings as they reformed, and the F-actin staining pattern was indistinguishable from that of control cells. (B, C) WAVE2 KD impairs junctional actin recovery after latrunculin washout. Representative confocal images of junctional F-actin (B) and quantitation of junctional fluorescence intensity (C) in control and WAVE2 KD cells. Data are n = 60 contacts for control and n = 58 contacts for WAVE2 KD from three independent experiments. Data are means ± SEM, normalized to control DMSO; *$p < 0.0001$. Scale bars, 10 μm.

contribute to supporting junctional tension. To extend this analysis, we then assessed tension in Arp3 KD cells; consistent with the effect of WAVE2, Arp3 depletion substantially reduced junctional tension compared with control junctions (Figure 6, G and H). Together these findings indicated that the WAVE2–Arp2/3 nucleator apparatus contributes to junctional tension at the ZA.

WAVE2 and Arp2/3 support junctional myosin II

Apical junctional tension is generally believed to be driven by myosin II–based contractility. Of the three myosin II proteins found in mammalian cells, myosin IIA and IIB localize to the ZAs of Caco-2 cells (Figure 7A), as they also do in MCF-7 cells (Smutny *et al.*, 2010). In contrast, junctional accumulation of both myosin IIA and IIB was significantly reduced in WAVE2 KD cells, accompanied by an increase in myosin staining on basal stress fibers (Figure 7, A and B, and Supplemental Figure S3). This suggested that dynamic actin assembly was necessary to support junctional accumulation of both these myosins. Consistent with this, junctional myosin IIA and IIB were also reduced in Arp3 siRNA cells (Figure 7C). In both experiments junctional myosin IIA was reduced to a greater extent than was junctional myosin IIB.

DISCUSSION

The zonula adherens appears to be a specialized junction where cell–cell adhesion is coupled to actomyosin to generate contractile tension (Sawyer *et al.*, 2010; Ratheesh *et al.*, 2012). However, the ZA cytoskeleton contains a high proportion of dynamic actin filaments, and its maintenance requires ongoing actin assembly (Kovacs *et al.*, 2011; Mangold *et al.*, 2011). This raises the question of whether actin assembly affects contractility and junctional tension at the ZA. Our current findings lead to three conclusions. First, the WAVE2–Arp2/3 apparatus is a major nucleator of actin assembly at the ZA. Second, this nucleator complex, and by implication the actin networks that it generates, is necessary for junctional tension. Finally, the WAVE2–Arp2/3 complex supports junctional tension by facilitating the recruitment of myosin II to the ZA. Together these suggest that a close relationship exists between Arp2/3-mediated actin assembly and myosin-driven contractility at the ZA.

WAVE2–Arp2/3 is a major nucleator of actin assembly at the ZA

The high rates of actin filament turnover at cadherin junctions strongly imply that ongoing assembly is necessary to maintain its steady-state F-actin content. Arp2/3 is one potential nucleator for junctional actin assembly, as it localizes to the ZA (Helwani *et al.*, 2004; Verma *et al.*, 2004; Kovacs *et al.*, 2011), possibly through a direct or indirect interaction with the E-cadherin molecular complex (Kovacs *et al.*, 2002). We now find that Arp3 RNAi reduces both actin nucleation and steady-state junctional F-actin content. Taken together with earlier experiments using drug (Kovacs *et al.*, 2011) or dominant-negative (Verma *et al.*, 2004) inhibitors, these establish Arp2/3 as a major contributor to actin filament homeostasis at these junctions. This is consistent with the recent demonstration that Arp2/3 was necessary for the junctional cytoskeleton to reassemble after latrunculin treatment (Tang and Brieher, 2012). These data do not exclude contributions from other nucleators, notably formins (Kobielak *et al.*, 2004; Carramusa *et al.*, 2007), but suggest that alternative nucleators cannot fully compensate when the activity of Arp2/3 is inhibited, either acutely or over more prolonged periods.

Our data further identify WAVE2 as a key part of this junctional actin nucleator apparatus. Arp2/3 is intrinsically inactive, and it is stimulated in response to cell signaling by intermediary proteins, notably the WASP/WAVE family (Padrick and Rosen, 2010). The Caco-2 cells used in our experiments express both N-WASP (Kovacs *et al.*, 2011) and WAVE2, with little, if any, mRNA for other WAVE proteins detectable. Although N-WASP supports the junctional actin cytoskeleton, it appears to act at a postnucleation step to stabilize filaments (Kovacs *et al.*, 2011). In contrast, WAVE2 depletion mimicked the effects of Arp3 RNAi, substantially reducing junctional nucleation and steady-state junctional F-actin content. This confirms and extends earlier work that identified WAVE2 as a regulator of junctional actin integrity in MDCK cells but did not assess actin nucleation directly (Yamazaki *et al.*, 2007). Furthermore, WAVE2 depletion reduced junctional Arp2/3, strengthening the notion that these proteins function together as a nucleator apparatus at the ZA. WAVE2 localization required E-cadherin, and association between

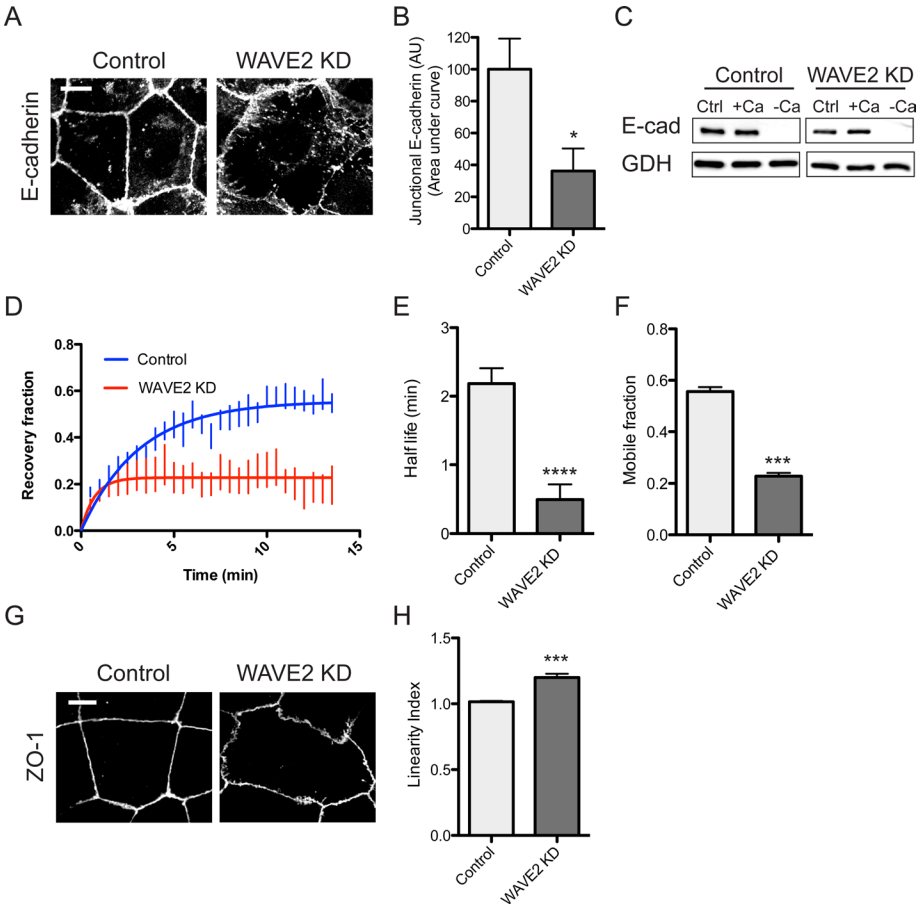

FIGURE 5: WAVE2 regulates E-cadherin organization and dynamics at the zonula adherens. (A, B) WAVE2 KD reduces apical concentration of E-cadherin into the ZA. Representative confocal immunofluorescence images of E-cadherin in control and WAVE2 KD cells (A) and quantitation by line scan analysis (B; $n = 20$ contacts from three independent experiments). (C) Total and surface E-cadherin (E-cad) levels in control and WAVE2 KD cells measured by sensitivity to digestion by extracellular trypsin in the presence or absence of Ca^{2+}. Results are representative of three independent experiments. Ctrl, no trypsin added; +Ca, trypsin added in media containing 2 mM Ca^{2+}; –Ca, trypsin added in calcium-free media. GAPDH (GDH) was used as a loading control. (D–F) FRAP of junctional E-cadherin–GFP expressed in E-cadherin shRNA cells ($n = 6$). Half-life of recovery (E) and mobile fraction (F) were reduced in WAVE2 KD cells. (G) Junctional linearity was reduced in WAVE2 KD cells, as revealed by immunostaining for ZO-1 and quantitated (H; linearity index) as described in *Materials and Methods*. Data are means ± SEM, normalized to controls; $n = 29$ for control and $n = 33$ for WAVE2 KD from three independent experiments; AU, arbitrary units; ***$p < 0.001$, ****$p < 0.0001$. Scale bars, 10 μm.

the two proteins was detectable by coimmunoprecipitation analysis. This biochemical interaction would allow actin assembly to be focused on cadherin adhesions. WAVE2 at the ZA appears to act downstream of Rac signaling and it is likely to respond as part of the wave regulatory complex. This emphasizes the central role that Rac plays in dynamic actin assembly at cadherin junctions (Braga *et al.*, 1997; Kraemer *et al.*, 2007), as it does at other subcellular locations (Steffen *et al.*, 2004; Padrick and Rosen, 2010).

WAVE2–Arp2/3 supports junctional tension at the ZA

The relationship between actin filament dynamics and contractility is complex. Arp2/3 can functionally constrain myosin II function (Yang *et al.*, 2012), suggesting that actin assembly may antagonize contractility; indeed, specialized contractile apparatuses, such as the sarcomeres of skeletal and cardiac muscle, are distinguished by apparently stable actin filament populations (Ono, 2010). Even in sarcomeres, however, actin filaments undergo turnover that can be promoted by increased contractility (Skwarek-Maruszewska *et al.*, 2009), implying that mechanisms must exist to sustain contractility despite filament turnover. In our experience, actin assembly and contractile tension both occur at the epithelial ZA (Verma *et al.*, 2004; Kovacs *et al.*, 2011; Ratheesh *et al.*, 2012), and our present findings demonstrate that Arp2/3 and WAVE2 are necessary to support junctional tension. Thus junctional tension, measured using laser nanoscissors, was substantially decreased by either Arp3 or WAVE2 RNAi. Similarly, WAVE2 depletion altered the normal linear morphology of apical junctions and decreased the ability of cells to buffer side-to-side movement at the junctions, both features consistent with decreased junctional tension (Otani *et al.*, 2006; Smutny *et al.*, 2011). Overall we conclude that ongoing actin assembly is necessary for tension to be generated at the ZA.

Dynamic actin assembly regulates myosin II recruitment

We further suggest that WAVE2–Arp2/3 promotes junctional tension by facilitating the recruitment of myosin II to the junction. This notion was prompted by the observation that myosin IIA and myosin IIB, which both contribute to junctional tension (Ratheesh *et al.*, 2012; Gomez and Yap, unpublished data), were reduced at junctions in WAVE2 or Arp3 KD cells, although total cellular levels of both proteins were unchanged (unpublished data). These findings add to the matrix of factors that influence the subcellular localization of myosin II. Known regulatory influences include signals such as the Rho-ROCK pathway and Rap1, which promote the accumulation of myosin IIA and myosin IIB at the ZA, respectively (Smutny *et al.*, 2010; McLachlan and Yap, 2011; Ratheesh *et al.*, 2012). We propose that local actin regulation collaborates with these signaling pathways to promote the robust recruitment of myosin II to the ZA. Similarly, actin network geometry and organization can affect the binding of other myosins (Nagy *et al.*, 2008; Brawley and Rock, 2009).

This raises the interesting question of whether filament branching by Arp2/3 substantively constrains myosin II recruitment or contractility. It is plausible to predict that branched actin networks would limit myosin II action at the ZA, based on evidence that Arp2/3 constrains myosin II–based cortical flow (Yang *et al.*, 2012) and that myosins can be excluded from Arp2/3-nucleated networks (Weinberg and Drubin, 2012). Our findings argue, however, that Arp2/3 ultimately promotes myosin II action at the ZA. One possibility is that network reorganization, potentially including debranching, occurs after nucleation to promote optimal myosin binding and contractility. The existence of reorganization might be inferred from earlier evidence that the apical actin rings of the ZA contain actin

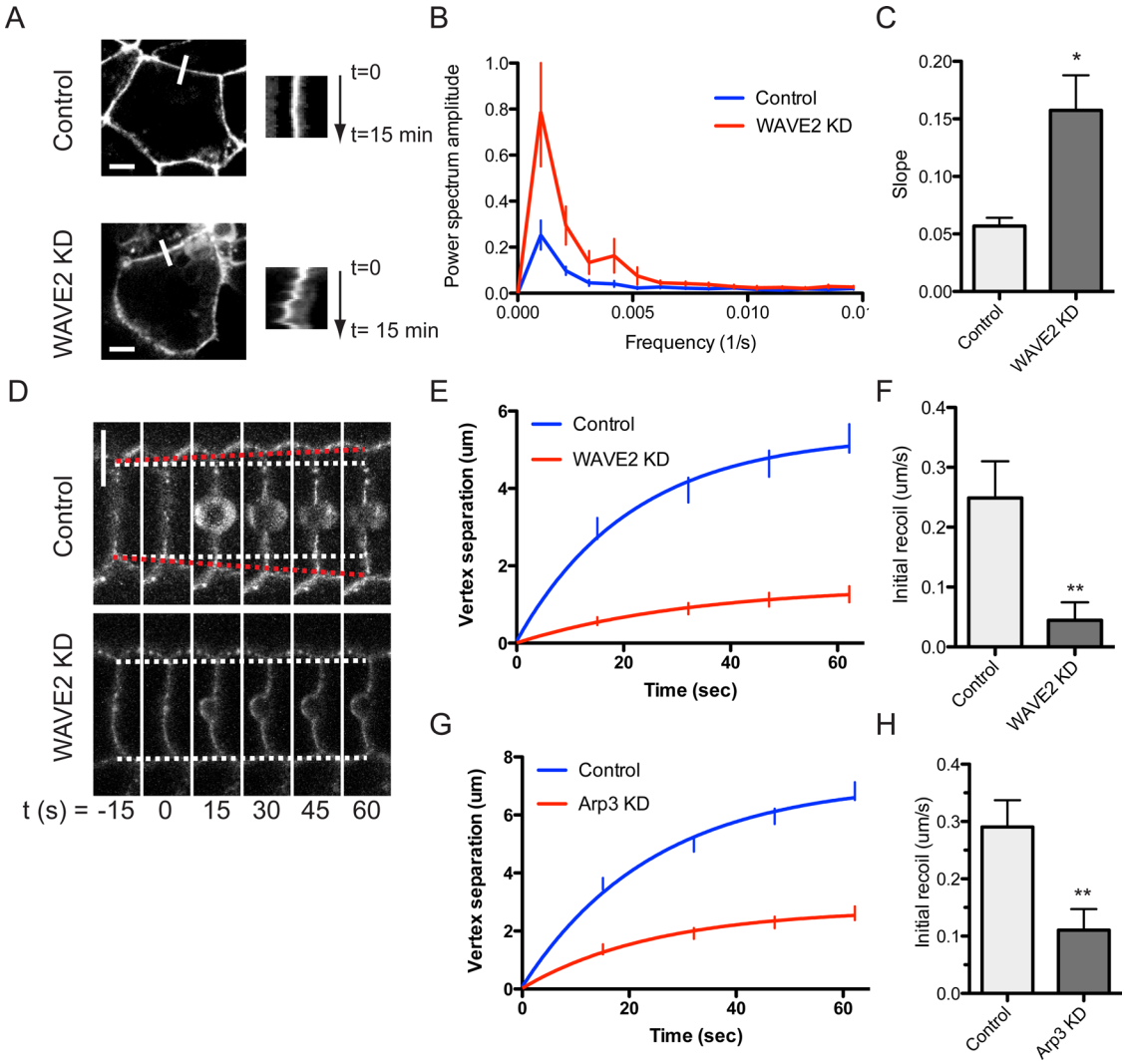

FIGURE 6: WAVE2–Arp2/3 regulate lateral junctional movement and tension at the zonula adherens. (A–C) WAVE2 KD increases lateral (orthogonal) junctional movement. E-cadherin–GFP at the ZA was recorded by time-lapse confocal imaging. Representative apical junction images (left) and kymographs (right, taken at the white bars) of control and WAVE2 KD cells are shown in A. (B) Power spectra of orthogonal movements from fast Fourier analysis of kymographs ($n = 4$). (C) Net translational movement of the apical junction was measured as described in *Materials and Methods* ($n = 4$). (D–H) WAVE2 and Arp3 KD reduce junctional tension at the ZA. Junctions were cut with laser nanoscissors and recoil of the E-cadherin-GFP vertices measured as an index of junctional tension. (D) Image sequence of contacts in control and WAVE2 KD cells undergoing laser ablation at $t = 0$. White dashed lines indicate starting positions of contact vertices; red dashed lines indicate expansion of control contact after laser ablation. Vertex separation was reduced in WAVE2 KD cells (E; $n = 27$ and 24 for control and KD cells, respectively) and in Arp3 KD cells (G; $n = 35$ and 30 for control and KD cells, respectively). Initial recoil, as measured by the instantaneous rate of vertex separation at $t = 0$, was reduced in WAVE2 KD (F) and Arp3 KD cells (H). Data are means ± SEM, normalized to controls; $*p < 0.05$, $**p < 0.01$. Scale bar, 10 μm.

bundles (Hirokawa *et al.*, 1983; Tepass and Hartenstein, 1994). Given that the actin rings in our cells were also depleted when the WAVE2–Arp2/3 apparatus was perturbed, we hypothesize that filaments in the rings might originally have been nucleated by Arp2/3 and subsequently remodeled to generate bundles. A cortical pool of filaments can be identified at the membrane (Zhang *et al.*, 2005), separable from the prominent apical cables (Kovacs *et al.*, 2011). It is tempting to hypothesize that these cortical filaments are the nascent products of Arp2/3 nucleation, which may serve to limit myosin II incorporation at the cortex itself. Subsequent filament reorganization may then generate bundles and allow myosin II incorporation. Testing this hypothesis will require ultrastructural characterization of actin organization in the apical rings in our cell systems, as well as analysis of postnucleation regulators, work that is ongoing in our laboratory.

Overall our findings identify WAVE2–Arp2/3 as necessary for myosin II recruitment and tension generation at the zonula adherens. We hasten to add, however, that not all the junctional effects of WAVE2–Arp2/3 can be explained by the recruitment of myosin II. Minimally, the contractile activity of myosins is generated by filament sliding. It is likely that loss of junctional filaments also contributed to the reduced junctional tension seen in WAVE2- or

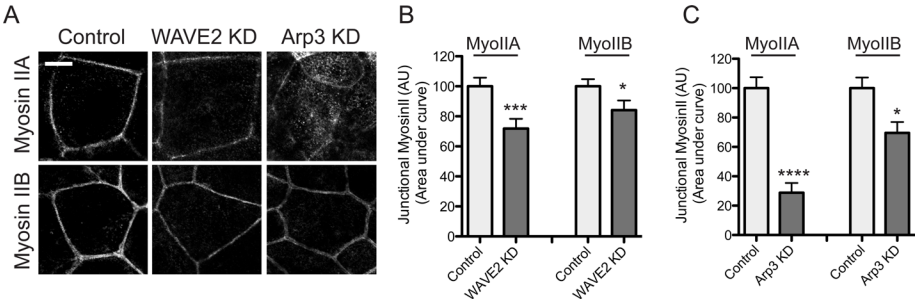

FIGURE 7: WAVE2 regulates junctional myosin II accumulation. (A) Representative apical junction staining for myosin IIA and myosin IIB in control, WAVE2 KD, and Arp3 KD cells. (B, C) Junctional concentration of myosin IIA and myosin IIB measured by line scan analysis of immunofluorescence intensity in WAVE2 KD (B) and Arp3 KD (C) cells. Data are means ± SEM, normalized to controls; $n = 52$ contacts from three independent experiments; *$p < 0.05$, ***$p < 0.001$, ****$p < 0.0001$; AU, arbitrary units. Scale bar, 10 μm.

Arp3-depleted cells. Nor are the junctional effects of WAVE2–Arp2/3 wholly attributable to the effect of junctional tension. Of note, we found that the unidirectional movement of the ZA from one side to another was more pronounced in WAVE2 KD cells, although myosin IIB depletion (which would reduce tension) decreased the rate of unidirectional movement (Smutny *et al.*, 2011). Instead, WAVE2-nucleated filaments may buffer junctional translocation by themselves acting as resistance elements and/or by anchoring other potential resistance elements, such as myosin VI (Maddugoda *et al.*, 2007). We add that, although we favor the notion that these orthogonal junctional movements reflect the mechanical effect of the junctional cytoskeleton, it remains possible that they are subject to forces generated elsewhere in the cell that are transmitted to the junctions.

Finally, it is noteworthy that E-cadherin mobility appeared to be decreased in FRAP studies. We interpret these FRAP analyses to reflect molecular movement or mobility of cadherin (within the membrane or by turnover) in contrast to the larger-scale movement of the whole ZA. Indeed, we tracked the sites of fluorescence recovery to ensure that we allowed for any junctional movement. Our findings thus suggest that WAVE2 supports a dynamic pool of cadherin at the ZA, which contrasts with the stabilization of cadherin mobility by myosin IIA (Ratheesh *et al.*, 2012). Arp2/3 has been implicated in clathrin-mediated endocytosis (Weinberg and Drubin, 2012), but whether turnover accounts for the effect of WAVE2 on E-cadherin dynamics remains to be examined.

In any case, our present findings emphasize that the junctional cytoskeleton is an integrated system in which filament dynamics is coordinated with motor action. These also involve an overlaid network of signals, including Rac, Rho, and Rap1 GTPases and Src kinase signaling, which have all been implicated in regulating different aspects of the junctional cytoskeleton (Braga *et al.*, 1997; Kraemer *et al.*, 2007; McLachlan and Yap, 2011). A deeper characterization of the junctional cytoskeleton will then entail understanding how these signals and effectors are integrated into a robust cellular system.

MATERIALS AND METHODS

Cell culture and transfections

Caco-2 cells were cultured in RPMI complete growth medium and grown at 37°C in 5% CO_2. Cells were transfected with Lipofectamine 2000 or Lipofectamine RNAiMAX (both from Invitrogen, Carlsbad, CA) according to manufacturer's instructions for plasmids or siRNAs, respectively.

Plasmids and RNAi

Myc-tagged DNRac in pCDNA3.1(+) was a kind gift from A. Hall (Sloan-Kettering Institute, New York, NY). DNcdc42 in EGFP-C1 was a kind gift from K. Kaibuchi (Nagoya University, Nagoya, Japan). To make WAVE2-mCherry and WAVE2-GFP, the human WAVE2 sequence was amplified and cloned into p-Cherry-N1 and pEGFP-N1 (both from Clontech, Mountain View, CA), respectively. The E-cadherin–GFP was expressed in E-cadherin short hairpin RNA cells using a lentivirus-based system, as described previously (Kovacs *et al.*, 2011; Smutny *et al.*, 2011). This resulted in simultaneous knockdown of endogenous E-cadherin and expression of RNAi-resistant E-cadherin–GFP at levels suitable for imaging. siRNAs used in this study were Dharmacon Smartpool RNAi duplexes against WAVE2 ORF (L-012141-00-0010), WAVE2 3′ UTR (J-012141-08), Arp3 (L-012081-00-0010), or control scrambled siRNA (D-001810-01-05; Dharmacon, Lafayette, CO). siRNAs were used at a final concentration of 100 nM.

Antibodies and immunoprecipitation

Primary antibodies used in this study were as follows: rabbit polyclonal against WAVE2 (1:50 for immunofluorescence [IF], 1:2000 for Western blot [WB]; Cell Signaling Technology, Beverly, MA), rabbit polyclonal against glyceraldehyde-3-phosphate dehydrogenase (GAPDH, 1:2000 WB; R&D, Minneapolis, MN), mouse monoclonal HECD-1 against ectodomain of E-cadherin (1:50 IF, 1:100 WB; kind gift from P. Wheelock, University of Nebraska, Omaha, NE, with the permission of M. Takeichi), mouse monoclonal against ZO-1 (1:100 IF; Invitrogen), mouse monoclonal against Rac1 (1:500 IF; Upstate Biotechnologies, Millipore, Billerica, MA), mouse monoclonal against Sra1 (1:50 IF; Sigma-Aldrich, St. Louis, MO), rabbit polyclonal against Nap1 (1:50 IF; Sigma-Aldrich), mouse monoclonal against Arp3 (1:50 IF; Sigma-Aldrich), mouse monoclonal against myosin IIA (1:600 IF; Abcam, Cambridge, MA), rabbit polyclonal against myosin IIA (1:400 IF; Sigma-Aldrich), mouse monoclonal against myosin IIB CMII26 (1:100 IF; Developmental Studies Hybridoma Bank, University of Iowa, Iowa City, IA), and rabbit polyclonal against myosin IIB (1:100 IF; Sigma-Aldrich). Secondary antibodies were species-specific antibodies conjugated with Alexa Fluor 488, 594, or 647 (Invitrogen) for immunofluorescence or with horseradish peroxidase (Bio-Rad, Hercules, CA) for immunoblotting. F-actin was stained using Alexa 488– or Alexa 594–phalloidin (1:500; Invitrogen).

Cells were lysed in 1 ml of lysis buffer (1% Nonidet P-40, 150 mM NaCl, 50 mM Tris-HCl, pH 7.4, 1 mM EDTA, 50 mM sodium fluoride, 2 mM sodium vanadate, 0.1% bovine serum albumin, and complete protease inhibitors [Roche Applied Science, Indianapolis, IN]). Immunoprecipitations were performed using ~1 mg of total protein, to which 2 μg of antibody and 20 μl of packed slurry of protein A–Sepharose beads (GE Healthcare, Piscataway, NJ) were added. Protein complexes were dissociated from beads, and samples were run on SDS–PAGE gels.

Real-time PCR

Total RNA was extracted from Caco-2 cell line using RNeasy Mini Kit (Qiagen, Valencia, CA) and was reverse transcribed using a SuperScript III First Strand Synthesis System (Life Technologies) as per the

manufacturer's instructions. cDNA samples were assayed by quantitative real-time PCR for Wasf1, Wasf2, and Wasf3 (WAVE1, WAVE2, and WAVE3, respectively) gene expression using inventoried TaqMan gene expression assays (Applied Biosystems, Foster City, CA; assay ID: Hs01591751_m1: Wasf1; Hs00819075_gH: Wasf2; Hs00903488_m1: Wasf3). Relative expression of Wasf1, Wasf2, and Wasf3 was normalized to housekeeping gene HPRT1 expression (assay ID: Hs01003267_m1) using a comparative method ($2-\Delta\Delta^{CT}$) according to the ABI relative quantitation guide.

Immunofluorescence microscopy and image analysis

For Rac and Cdc42 immunostaining, cells were fixed in 10% trichloroacetic acid for 10 min. For all other stainings, cells were fixed with 4% paraformaldehyde in cytoskeletal stabilization buffer (10 mM 1,4-piperazinediethanesulfonic acid at pH 6.8, 100 mM KCl, 300 mM sucrose, 2 mM ethylene glycol tetraacetic acid [EGTA], and 2 mM $MgCl_2$) on ice for 20 min. Fixed coverslips were then permeabilized with 0.25% Triton X-100 in phosphate-buffered saline for 10 min at room temperature. Confocal images were acquired on a Zeiss LSM710 microscope (Carl Zeiss, Jen, Germany) and processed using ImageJ (National Institutes of Health, Bethesda, MD) and Photoshop (Adobe, San Jose, CA).

Quantitative analysis of staining intensity at contacts was performed in ImageJ with the line scan function, as previously described (Smutny *et al.*, 2010). Briefly, a line of length 40 pixels was selected centered on and perpendicular to a contact. The PlotProfile feature was used to record the pixel intensities along the selected line, and the data were imported into Prism 5 (GraphPad Software, La Jolla, CA). Pixel intensity was corrected for background, and a Gaussian curve was fitted to each intensity profile, from which the mean and SD of the maximum heights were calculated. For the latrunculin assay, a region of interest spanning each contact was drawn using the 10-pixel-wide ImageJ freehand line tool. The mean phalloidin intensity for each region of interest was then measured.

Assays

The latrunculin washout assay was a modification of a recently described protocol (Tang and Brieher, 2012). Caco-2 cells were transfected with control or WAVE2 siRNA oligos, plated onto glass coverslips, and grown to confluency. Coverslips were then treated with 1 µM latrunculin A (Sigma-Aldrich) for 2 h. Cells were rinsed twice and incubated with cell growth media for 0–60 min, after which they were processed for immunostaining as described.

Barbed ends were labeled by G-actin incorporation (Kovacs *et al.*, 2011). Confluent monolayers of Caco-2 cells were permeabilized with saponin for 7 min in the presence of 0.45 µM Alexa 594–tagged G-actin to favor barbed-end incorporation. Cells were then fixed in 4% paraformaldehyde in cytoskeletal stabilization buffer containing 2% Triton X-100 and Alexa 488–phalloidin (1:500). Surface E-cadherin was measured by sensitivity to surface trypsin digestion (Verma *et al.*, 2004). Briefly, lysates were prepared from monolayers that were untreated (control) or trypsinized in the presence of 2 mM $CaCl_2$ (+Ca) or in the absence of 2 mM $CaCl_2$ and presence of 2 mM EGTA (–Ca). Samples were run on SDS–PAGE gels and probed with antibodies directed against the ectodomain of human E-cadherin (HECD-1) or GAPDH as a loading control.

Live-cell imaging

Analysis of contact movements. Cells were grown on glass-bottomed dishes (In Vitro Scientific, Sunnyvale, CA), and live-cell imaging was performed on a spinning-disk confocal system (Ultra-View; PerkinElmer, Waltham, MA) mounted on an IX81 Olympus microscope (Olympus, Tokyo, Japan) with ×60 and ×100/1.40 numerical aperture Plan Apochromat objectives and an Orca-1 ER camera (Hamamatsu, Hamamatsu, Japan) driven by MetaMorph imaging software, version 7 (Molecular Devices, Sunnyvale, CA). Kymographs were generated using the Multiple Kymograph function in ImageJ. Contact movement in E-cadherin-GFP–expressing cells was quantitated as previously described (Smutny *et al.*, 2011). Briefly, movies were processed by drawing a line perpendicular to a contact, and the position along the line at which the maximum intensity occurred was recorded for each time frame using an ImageJ script. The translational component was obtained by calculating the slope of the best-fit line to the position of maxima over time. The oscillatory component was then obtained by subtracting the translational component from the positional data and then decomposing the result into its frequency components by fast Fourier transform.

FRAP experiments. FRAP experiments were performed with a Zeiss LSM510 microscope (Carl Zeiss, Jena, Germany) with a heated stage maintained at 37°C. Images were acquired using a 100× objective/1.4 numerical aperture oil Plan Apochromat immersion lens, and E-cadherin–GFP at contacts was photobleached using a constant region of interest (ROI) using a 488-nm laser with its transmission set to 100%. Recovery in the photobleached area was tracked from frame to frame to correct for movement of the overall junction. Fluorescence intensity profiles were corrected for acquisition photobleaching and normalized to prebleach values as previously described (Kovacs *et al.*, 2011). Normalized FRAP curves were fitted to a recovery curve using Prism to calculate half-times of recovery and plateau levels (Ratheesh *et al.*, 2012).

Laser nanoscissors. Localized ablation of a small region of cell–cell contacts in E-cadherin–expressing cells was performed as previously described (Ratheesh *et al.*, 2012). Briefly, experiments were performed on a Zeiss LSM 510 confocal microscope at 37°C. Images were acquired using a 63× objective, 1.4 numerical aperture oil Plan Apochromat immersion lens at 1.5× digital magnification and pinhole adjusted to 3 Airy units to obtain a 2-µm optical section. For ablation, a Ti:sapphire laser (Chameleon Ultra; Coherent Scientific, Santa Clara, CA) tuned to 790 nm was used to ablate cell contacts labeled with E-cadherin–GFP. A constant ROI was marked for each experiment and ablated with 30 iterations of the 790-nm laser with 50% transmission. GFP fluorescence was determined before (three frames) and after (four frames) ablation with an interval of 15 s per frame, using a 488-nm laser for excitation and a 500- to 550-nm emission filter. Image analysis was performed using ImageJ. The distance, d, between vertices that defined the ablated contact was measured as a function of time, t. Next the average distance before the ablation step, $d(0)$, was subtracted from the distance values, and the resulting values were plotted and fitted to the following equation:

$$d(t) - d(0) = \text{plateau} \cdot (1 - e^{-kt})$$

where k is the rate constant. The instantaneous recoil (rate of recoil at $t = 0$ s) was determined as

$$\text{Instantaneous recoil} = \text{plateau} \cdot k$$

Average instantaneous recoil was determined for 30–50 contacts in three independent experiments and then normalized to the value observed in control conditions.

ACKNOWLEDGMENTS

We thank our colleagues for gifts of reagents and all the members of our lab for their thoughtful suggestions and support. This work was supported by the National Health and Medical Research Council of Australia (63137), the Australian Research Council (DP120104667), the Human Frontiers Science Program, and the Kids Cancer Project of the Oncology Children's Foundation. A.S.Y. (631383) and R.D.T. (511042) are Research Fellows of the National Health and Medical Research Council (Australia). Confocal imaging was performed at the Institute for Molecular Bioscience/Australian Cancer Research Foundation Cancer Biology Imaging Facility, established with the generous support of the Australian Cancer Research Foundation.

REFERENCES

Berger S, Schafer G, Kesper DA, Holz A, Eriksson T, Palmer RH, Beck L, Klambt C, Renkawitz-Pohl R, Onel SF (2008). WASP and SCAR have distinct roles in activating the Arp2/3 complex during myoblast fusion. J Cell Sci 121, 1303–1313.

Braga VMM, Machesky LM, Hall A, Hotchin NA (1997). The small GPTases rho and rac are required for the formation of cadherin-dependent cell-cell contacts. J Cell Biol 137, 1421–1431.

Brawley CM, Rock RS (2009). Unconventional myosin traffic in cells reveals a selective actin cytoskeleton. Proc Natl Acad Sci USA 106, 9685–9690.

Carramusa L, Ballestrem C, Zilberman Y, Bershadsky AD (2007). Mammalian diaphanous-related formin Dia1 controls the organization of E-cadherin-mediated cell-cell junctions. J Cell Sci 120, 3870–3882.

Clark K, Langeslag M, Figdor CG, van Leeuwen FN (2007). Myosin II and mechanotransduction: a balancing act. Trends Cell Biol 17, 178–186.

Fernandez-Gonzalez R, Simoes Sde M, Roper JC, Eaton S, Zallen JA (2009). Myosin II dynamics are regulated by tension in intercalating cells. Dev Cell 17, 736–743.

Helwani FM, Kovacs EM, Paterson AD, Verma S, Ali RG, Fanning AS, Weed SA, Yap AS (2004). Cortactin is necessary for E-cadherin-mediated contact formation and actin reorganization. J Cell Biol 164, 899–910.

Hirokawa N, Keller TC 3rd, Chasan R, Mooseker MS (1983). Mechanism of brush border contractility studied by the quick-freeze, deep-etch method. J Cell Biol 96, 1325–1336.

Insall RH, Machesky LM (2009). Actin dynamics at the leading edge: from simple machinery to complex networks. Dev Cell 17, 310–322.

Ivanov AI, Hunt D, Utech M, Nusrat A, Parkos CA (2005). Differential roles for actin polymerization and a myosin II motor in assembly of the epithelial apical junctional complex. Mol Biol Cell 16, 2636–2650.

Kim SH, Li Z, Sacks DB (2000). E-cadherin-mediated cell-cell attachment activates Cdc42. J Biol Chem 275, 36999–37005.

Kobielak A, Pasolli HA, Fuchs E (2004). Mammalian formin-1 participates in adherens junctions and polymerization of linear actin cables. Nat Cell Biol 6, 21–30.

Kovacs EM, Goodwin M, Ali RG, Paterson AD, Yap AS (2002). Cadherin-directed actin assembly: E-cadherin physically associates with the Arp2/3 complex to direct actin assembly in nascent adhesive contacts. Curr Biol 12, 379–382.

Kovacs EM, Verma S, Ali RG, Ratheesh A, Hamilton NA, Akhmanova A, Yap AS (2011). N-WASP regulates the epithelial junctional actin cytoskeleton through a non-canonical post-nucleation pathway. Nat Cell Biol 13, 934–943.

Kraemer A, Goodwin M, Verma S, Yap AS, Ali RG (2007). Rac is a dominant regulator of cadherin-directed actin assembly that is activated by adhesive ligation independently of Tiam1. Am J Phys 292, C1061–C1069.

Loveless T, Hardin J (2012). Cadherin complexity: recent insights into cadherin superfamily function in *C. elegans*. Curr Opin Cell Biol 24, 695–701.

Maddugoda MP, Crampton MS, Shewan AM, Yap AS (2007). Myosin VI and vinculin cooperate during the morphogenesis of cadherin cell-cell contacts in mammalian epithelial cells. J Cell Biol 178, 529–540.

Mangold S, Wu SK, Norwood SJ, Collins BM, Hamilton NA, Thorn P, Yap AS (2011). Hepatocyte growth factor acutely perturbs actin filament anchorage at the epithelial zonula adherens. Curr Biol 21, 503–507.

McLachlan RW, Yap AS (2011). Protein tyrosine phosphatase activity is necessary for E-cadherin-activated Src signaling. Cytoskeleton (Hoboken) 68, 32–43.

Michelot A, Drubin DG (2011). Building distinct actin filament networks in a common cytoplasm. Curr Biol 21, R560-R569.

Muller HA, Wieschaus E (1996). armadillo, bazooka, and stardust are critical for early stages in formation of the zonula adherens and maintenance of the polarized blastoderm epithelium in *Drosophila*. J Cell Biol 134, 149–163.

Nagy S, Ricca BL, Norstrom MF, Courson DS, Brawley CM, Smithback PA, Rock RS (2008). A myosin motor that selects bundled actin for motility. Proc Natl Acad Sci USA 105, 9616–9620.

Ono S (2010). Dynamic regulation of sarcomeric actin filaments in striated muscle. Cytoskeleton (Hoboken) 67, 677–692.

Otani T, Ichii T, Aono S, Takeichi M (2006). Cdc42 GEF Tuba regulates the junctional configuration of simple epithelial cells. J Cell Biol 175, 135–146.

Padrick SB, Rosen MK (2010). Physical mechanisms of signal integration by WASP family proteins. Annu Rev Biochem 79, 707–735.

Ratheesh A, Gomez GA, Priya R, Verma S, Kovacs EM, Jiang K, Brown NH, Akhmanova A, Stehbens SJ, Yap AS (2012). Centralspindlin and a-catenin regulate Rho signalling at the epithelial zonula adherens. Nat Cell Biol 14, 818–828.

Reymann AC, Boujemaa-Paterski R, Martiel JL, Guerin C, Cao W, Chin HF, De La Cruz EM, Thery M, Blanchoin L (2012). Actin network architecture can determine myosin motor activity. Science 336, 1310–1314.

Sawyer JM, Harrell JR, Shemer G, Sullivan-Brown J, Roh-Johnson M, Goldstein B (2010). Apical constriction: a cell shape change that can drive morphogenesis. Dev Biol 341, 5–19.

Skwarek-Maruszewska A, Hotulainen P, Mattila PK, Lappalainen P (2009). Contractility-dependent actin dynamics in cardiomyocyte sarcomeres. J Cell Sci 122, 2119–2126.

Smutny M, Cox HL, Leerberg JM, Kovacs EM, Conti MA, Ferguson C, Hamilton NA, Parton RG, Adelstein RS, Yap AS (2010). Myosin II isoforms identify distinct functional modules that support integrity of the epithelial zonula adherens. Nat Cell Biol 12, 696–702.

Smutny M, Wu SK, Gomez GA, Mangold S, Yap AS, Hamilton NA (2011). Multicomponent analysis of junctional movements regulated by myosin II isoforms at the epithelial zonula adherens. PLoS ONE 6, e22458.

Steffen A, Rottner K, Ehinger J, Innocenti M, Scita G, Wehland J, Stradal TE (2004). Sra-1 and Nap1 link Rac to actin assembly driving lamellipodia formation. EMBO J 23, 749–759.

Takeichi M (1977). Functional correlation between cell adhesive properties and some cell surface proteins. J Cell Biol 75, 464–474.

Tang VW, Brieher WM (2012). alpha-Actinin-4/FSGS1 is required for Arp2/3-dependent actin assembly at the adherens junction. J Cell Biol 196, 115–130.

Tepass U, Hartenstein V (1994). The development of cellular junctions in the *Drosophila* embryo. Dev Biol 161, 563–596.

Verkhovsky AB, Svitkina TM, Borisy GG (1995). Myosin II filament assemblies in the active lamella of fibroblasts: their morphogenesis and role in the formation of actin filament bundles. J Cell Biol 131, 989–1002.

Verma S, Shewan AM, Scott JA, Helwani FM, Elzen NR, Miki H, Takenawa T, Yap AS (2004). Arp2/3 activity is necessary for efficient formation of E-cadherin adhesive contacts. J Biol Chem 279, 34062–34070.

Vicente-Manzanares M, Ma X, Adelstein RS, Horwitz AR (2009). Non-muscle myosin II takes centre stage in cell adhesion and migration. Nat Rev Mol Cell Biol 10, 778–790.

Weinberg J, Drubin DG (2012). Clathrin-mediated endocytosis in budding yeast. Trends Cell Biol 22, 1–13.

Yamazaki D, Oikawa T, Takenawa T (2007). Rac-WAVE-mediated actin reorganization is required for organization and maintenance of cell-cell adhesion. J Cell Sci 120, 86–100.

Yang Q, Zhang XF, Pollard TD, Forscher P (2012). Arp2/3 complex-dependent actin networks constrain myosin II function in driving retrograde actin flow. J Cell Biol 197, 939–956.

Yap AS, Brieher WM, Pruschy M, Gumbiner BM (1997). Lateral clustering of the adhesive ectodomain: a fundamental determinant of cadherin function. Curr Biol 7, 308–315.

Zhang J, Betson M, Erasmus J, Zeikos K, Bailly M, Cramer LP, Braga VM (2005). Actin at cell-cell junctions is composed of two dynamic and functional populations. J Cell Sci 118, 5549–5562.